

# Electrooptic Tuning of InP-Based Microphotonic Fabry–Pérot Filters

Maria V. Kotlyar, Liam O’Faolain, Andrey B. Krysa, and Thomas F. Krauss

**Abstract**—This paper presents the experimental results for compact (20- and 40- $\mu\text{m}$ -long) electrooptically tuned deeply etched Fabry–Pérot (F–P) filters in InP-based material. Both the quantum-confined Stark effect (QCSE) and carrier-injection (C-I) effects were implemented to achieve tunability of these microcavity filters. Red and blue shifts of the transmission peaks in the order of 1 to 2 nm were observed for both effects, and the limitations on C-I due to thermal effect are clearly demonstrated and discussed. The advantages and disadvantages of both tuning mechanisms are highlighted.

**Index Terms**—Fabry–Pérot (F–P) cavity, InP–InGaAsP, microresonators, quantum-confined Stark effect (QCSE), quantum-well (QW) devices, tunable filters.

## I. INTRODUCTION

**T**UNABILITY of compact devices is essential for the realization of microphotonic circuits. III–V semiconductors offer an attractive material platform in this respect, especially since InP gives access to several electrooptic effects and provides gain at the telecommunications wavelengths of 1.3 and 1.55  $\mu\text{m}$ .

The use of microcavities such as microrings [1], microdiscs [2], and Fabry–Pérot (F–P)-type resonators [3] allows for the confinement of the optical mode to very small regions. Thus, microcavity-based devices typically consume only small levels of external power to produce the desired tunability and can be potentially very fast due to small parasitic capacitances. The most common ways of realizing tunability in photonics are the quantum-confined Stark effect (QCSE), carrier injection (C-I), thermal tuning, and the Kerr effect. Of these, QCSE and C-I are the most promising in the microphotonics context; ultrafast tuning via the Kerr effect provides too small a refractive-index change, whereas thermal tuning is typically too slow (microsecond regime) and generates excessive heat loads for densely integrated circuits. The present paper therefore focuses on QCSE and C-I.

These effects cannot be considered in isolation, however; thermal effects are especially relevant for C-I devices, because carrier-related heating leads to the thermo-optic refractive-index shift that is of the opposite sign to the electrooptic shift [3]. Electrooptic and thermal effects may therefore cancel one

another, which is highly undesirable. Thermal conductivity is, thus, another reason for choosing a III–V substrate (as opposed to  $\text{SiO}_2$  or air claddings as in silicon-on-insulator (SOI) and membrane-type devices, respectively, both of which lead to much higher thermal impedances).

A further advantage of microcavities is that their transmission at the resonance wavelength becomes very sensitive to small refractive-index changes, so cavities with a high  $Q$  factor are preferable, especially for applications in switching.

The etching of high-aspect-ratio features in InP in order to create F–P-type microcavities is critical and very demanding. Two etching methods (inductively coupled plasma (ICP) and chemically assisted ion beam etching (CAIBE)) [4], [5] have recently been proven successful for this purpose, however. For example, we have already fabricated and characterized low-loss ( $\approx 2$  dB/mm) InP photonic-crystal waveguides using the CAIBE technique [6].

This paper reports the characteristics of tunable InP-based filters of the F–P resonator type using a small number of deeply etched air slots to form highly reflecting Bragg mirrors. Red and blue shifts of resonance transmission peaks were observed for QCSE- and C-I tuned devices, respectively. The tuning results are analyzed, highlighting the advantages and disadvantages of both mechanisms, as well as limitations due to carrier-induced heating. Critical aspects of these electrooptically tuned microcavities are then discussed.

## II. DEVICE DESIGN

Passive filters suitable for communications applications require a full-width at half-maximum (FWHM) of less than 2 nm, large free spectral ranges (FSRs) ( $> 10$  nm), and high transmitted power (close to 100%).

We consider an F–P resonator with deeply etched one-dimensional photonic-crystal mirrors [7]. Using such Bragg mirrors at the traditional “ $\lambda/4$ ” criterion would result in very high losses due to diffraction and out-of-plane scattering in the air sections. Due to the very high refractive-index contrast achievable in these deeply etched structures, however, one can deviate from the  $\lambda/4$  condition and still obtain high reflectivity and bandwidth ( $\approx 250$  nm). Thus, we choose a third-order stopband with air slots of 100 nm according to

$$l_1 n_1 + l_2 n_2 = \frac{3\lambda}{2} \quad (1)$$

where  $l_{1,2}$  is the length of the air/semiconductor section, and  $n_{1,2}$  is the refractive index in the air/semiconductor section. The minimum cavity length is  $\lambda/2$ , but for practical purposes, i.e., in order to allow electrical contacting, we have chosen a longer

Manuscript received December 15, 2004; revised February 17, 2005.

M. V. Kotlyar, L. O’Faolain, and T. F. Krauss are with the School of Physics and Astronomy, University of St. Andrews, St. Andrews, Fife KY 16 9SS, Scotland, U.K. (e-mail: mvk@st-andrews.ac.uk; jww1@st-andrews.ac.uk; tfk@st-andrews.ac.uk).

A. B. Krysa is with the Engineering and Physical Sciences Research Council (EPSRC) National Centre for III–V Technologies, University of Sheffield, Sheffield S1 3JD, U.K. (e-mail: a.krysa@sheffield.ac.uk).

Digital Object Identifier 10.1109/JLT.2005.849880

TABLE I  
 WAFER DESIGNS FOR C-I (WAFER A) AND QCSE (WAFER B)

Wafer A			Wafer B		
Repeat	Thickness, nm	Material (C-I)	Repeat	Thickness, nm	Material (QCSE)
1	10	InGaAs			
1	600	InP	1	600	InP
1	150	InGaAsP(Q1.02)	1	354	InGaAsP(Q1.1)
1	8	InGaAsP(Q1.1)	1	76	InGaAsP(Q1.1)
5	6.5	InGaAsP(Q1.3)	10	6	InGaAsP(Q1.3)
5	8	InGaAsP(Q1.1)	10	76	InGaAsP(Q1.1)
1	150	InGaAsP(Q1.02)	1	430	InGaAsP(Q1.1)
1	700	InP	1	1500	InP

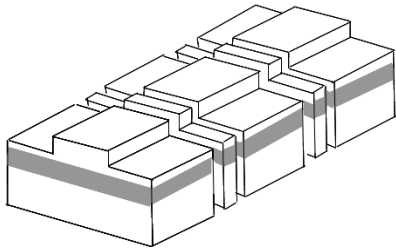


Fig. 1. Schematic view of the F-P-type filter with two InP-air Bragg mirrors (gray color indicates the waveguide core).

cavity of 20  $\mu\text{m}$  length with two air-InP Bragg mirrors. Three-dimensional (3-D) modeling (FIMMPROP by Photon Design) indicated an FSR of 12 nm and an FWHM of 1.1 nm.

This basic filter design (Fig. 1) is used for both the QCSE-based and the C-I-based tunable filters.

### III. MATERIAL DESIGN

The QCSE relies on an electric field applied perpendicular to the plane of a quantum well (QW), which induces changes in the absorption spectrum [8]. These changes are connected to changes in the refractive index via the Kramers-Kronig relationship [9] and, hence, allow tuning of the cavity resonance. Alternatively, C-I [10], via a forward bias, generates gain, which again translates into refractive-index change via the Kramers-Kronig relationship. In addition, free carriers change the material polarizability, and thereby the refractive index, via the plasma effect.

Two wafers were designed in order to study these effects in a microcavity context. The two wafer designs are detailed in Table I.

The ten-QW material was designed primarily for the QCSE experiments. The applied field causes the refractive index to change equally in all wells; thus, the larger number of wells gives a larger overall modal refractive-index change. A similar situation is, of course, true for C-I; however, the injection of carriers evenly into active layers with large numbers of QWs is complicated, leading to an uneven distribution [11], and thus a five-QW material was chosen.

Both materials have a bandgap at around 1240 nm. The QWs in wafer B (intended for QCSE) were evenly distributed in an 820-nm region of the core (the overall core thickness was 1.6  $\mu\text{m}$ ) using thick barriers of 76 nm. This distribution (as well as the thick core) leads to a “flat” waveguide mode with low numerical aperture, which helps to minimize diffraction losses

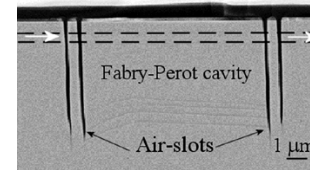


Fig. 2. Scanning electron microscope (SEM) image of the cross section of a 10- $\mu\text{m}$ -long cavity illustrating deeply etched (CAIBE) air slots reaching an aspect ratio of 35:1 (white arrows indicate the direction of light propagation).

at the air-semiconductor interface of the mirrors. It has been shown theoretically that weak confinement in the waveguide minimizes diffraction losses of deeply etched photonic crystals [12]. To emphasize this point, the low-loss two-dimensional (2-D) photonic-crystal waveguides we have recently reported were fabricated in this material [6].

Such thick barriers are not acceptable for wafer A (C-I) as they make the sweeping out of carriers difficult and consequently slower.

### IV. FILTER FABRICATION

The 100-nm air slots were electron-beam written in a 200-nm-thick layer of polymethylmethacrylate (PMMA). They were transferred into an  $\text{SiO}_2$  hard mask using reactive ion etching (RIE) with fluorine chemistry. Using a previously reported [5] CAIBE technique for etching high-aspect ratio features in InP-based material, deep straight air slots were etched with aspect ratios of approximately 35:1 (Fig. 2). A depth of  $>3.5 \mu\text{m}$  was essential as wafer B has a thick waveguide core of 1.6  $\mu\text{m}$ .

A second stage shallow etch (CAIBE) was used to create single-mode waveguides. Contact insulation pads were made from SU-8 polymer. Top and bottom contacts (Ni-Au and Au-Ge-Ni-Au, respectively) were then deposited using an electron beam evaporator. An SEM image giving a plan view of the QCSE device is presented in Fig. 3.

Square contact pads were used for C-I due to the fact that some of the “T-shaped” contacts burnt out at the interface between the insulated and the noninsulated section under forward biases.

### V. RESULTS: QCSE

A tunable laser operating between 1250–1365 nm was used to launch light into the device via an optical fiber. The substrate was mounted on an aluminum heat-sink using silver epoxy.

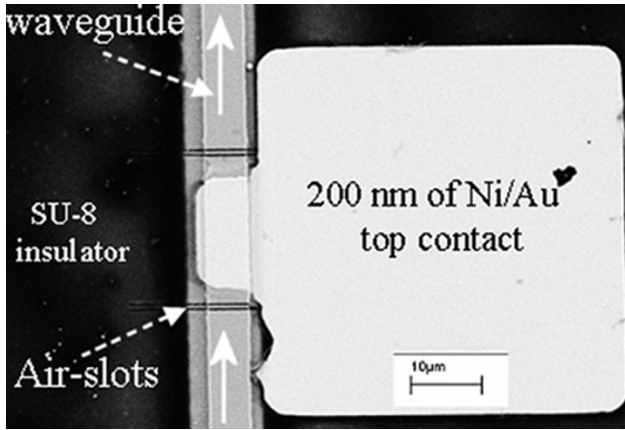


Fig. 3. SEM image of the top view of the QCSE-based tunable filter with “T-shaped” contacts (white arrows indicate the direction of light propagation).

The output light was collected via a microscope lens and passed through a polarizer (to select the TE polarization) before reaching the detector.

As the top and bottom claddings are doped, an applied electric field essentially drops across the intrinsic layer (1.6  $\mu\text{m}$  thick). When applying a reverse bias of 8 V, we observed a red shift of the resonator peaks (see Fig. 4). Red shifts of 1.6 and 0.9 nm were obtained at 1265 and 1285 nm, respectively.

The increasing height of the resonator peaks for longer wavelengths is due to the decreasing absorption of QWs away from the band edge. The closer to the band edge, the bigger the shift, as one can see from the figure. Therefore, there is an obvious tradeoff between maximizing refractive-index changes and minimizing absorption losses.

The electrooptic behavior of the device can be described by the following figure of merit [13]:

$$\eta = \Delta n \Delta \omega / E^2 \quad (2)$$

where  $\Delta \omega$  is the energy detuning from the bandgap,  $\Delta n$  is the refractive-index change, and  $E$  is the applied electric field.

This parameter can be useful for the prediction of changes in refractive index for different wavelengths and/or applied voltages. In our case, we found the electrooptic parameter to be  $4 \times 10^{-5} \text{ meV cm}^2 \text{ kV}^{-2}$ , using the shift of the resonator peak at a wavelength of 40 meV below the gap (corresponding to a wavelength of 1285 nm) and an applied voltage of 8 V.

Using this electrooptic parameter, we can express the refractive-index change as a function of the applied electric field. Fig. 5 shows a comparison between predicted and experimental data at a wavelength of 1310 nm. It is useful to note that even when applying 60 kV/cm across the active layer, the increase in the absorption-related loss was not prohibitive, resulting in a  $\Delta n / \Delta k$  of more than 20, where  $\Delta k$  is the QCSE-induced change in the extinction coefficient.

For the best device, this electrooptic parameter was improved by a factor of three, reaching a value of  $14 \times 10^{-5} \text{ meV cm}^2 \text{ kV}^{-2}$ . This parameter was calculated from an experimental shift of 1.2 nm at  $E = 37.5 \text{ kV/cm}$  and  $\Delta \omega = 64 \text{ meV}$  (see the insert in Fig. 4). This means that the previously mentioned value was not limited by the QW structure design but rather by fabrication imperfections. Using this parameter, we can predict a shift as

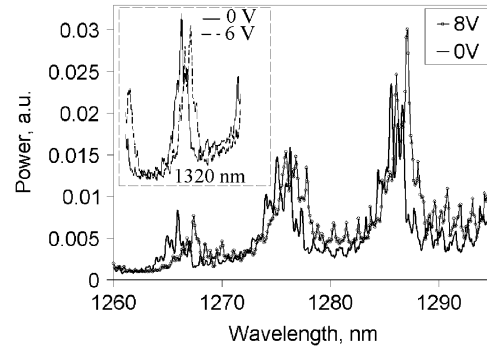


Fig. 4. Red shifts induced via QCSE at 50 kV/cm at different wavelengths. The filter has a cavity length of 20  $\mu\text{m}$ . The inset shows the red shift (1.2 nm) obtained at 1320 nm for an improved device at only 38 kV/cm.

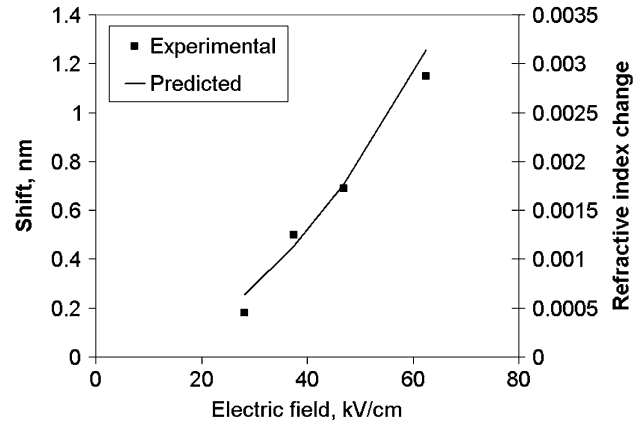


Fig. 5. Predicted and experimental modal refractive-index changes as a function of an electric field at 1310 nm.

big as 5 nm at the wavelength of 1265 nm, applying only  $E = 50 \text{ kV/cm}$ .

The refractive-index change  $\Delta n$  in (2) depends on the electric field via linear ( $r$ ) and quadratic ( $s$ ) electrooptic coefficients as follows [9], [13]:

$$\Delta n = -\frac{1}{2} n_0^3 (rE + sE^2) \quad (3)$$

where  $n_0$  is the refractive index in the absence of an applied electric field.

Bearing in mind that the linear dependence of the refractive index on the electric field is weak, we can neglect it in order to find the quadratic electrooptic coefficient either using (2) and (3) or as a fitting parameter in Fig. 5.

We found  $s$  to be  $-4 \times 10^{-14} \text{ cm}^2/\text{V}^2$  for an energy detuning of 60 meV from the band edge. This value compares favorably to the value of  $-1 \times 10^{-14} \text{ cm}^2/\text{V}^2$  reported in a ring resonator configuration also at 60 meV from the band edge reported elsewhere [14]. For comparison, a quadratic electrooptic coefficient of  $-2 \times 10^{-14} \text{ cm}^2/\text{V}^2$  was obtained experimentally for filters fabricated in wafer A (at  $\Delta \omega = 48 \text{ meV}$ ).

At an applied field of 62 kV/cm and  $\Delta \omega = 60 \text{ meV}$  (see Fig. 5), an efficiency of  $\Delta n / E = 460 \times 10^{-12} \text{ m/V}$  was found experimentally. This is of the same order as results reported elsewhere ( $\Delta n / E = 730 \times 10^{-12} \text{ m/V}$ ) but for wavelengths closer to the band edge ( $\Delta \omega = 44 \text{ meV}$ ) and at higher applied fields ( $E = 100 \text{ kV/cm}$ ) [13].

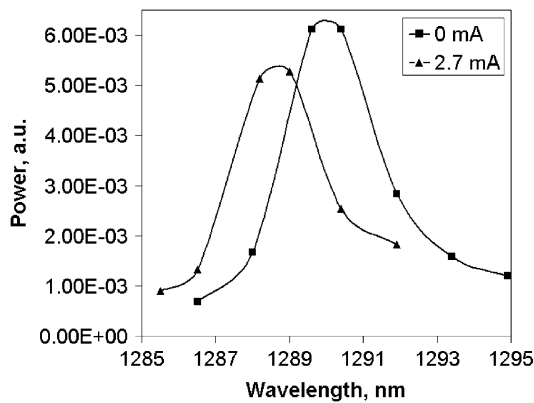


Fig. 6. Blue shift of 1.5 nm was observed for an injected current of 2.7 mA. The filter has a cavity length of 20  $\mu\text{m}$ .

## VI. RESULTS: CARRIER INJECTION

Our experiments on C-I-based tunable filters are described in more detail elsewhere [15]. The main point of this section is therefore to highlight the method's abilities and limitations and to compare them to QCSE-based tunability.

Applying a forward bias to the cavity creates carriers that relax into the QWs. These carriers cause changes in the absorption spectrum via band filling, bandgap shrinkage, and free-carrier absorption. Changes in the refractive index of the QWs result from these absorption spectrum changes and are governed by the Kramers–Kronig relationship. For carrier densities of around  $3 \times 10^{18}/\text{cm}^3$  and energies close to the bandgap, the band-filling effect is predominant and provides the largest contribution to the refractive-index changes.

Devices with two different cavities lengths of 20 and 40  $\mu\text{m}$  were examined. Blue shifts of 1.5 nm (at 1290 nm) and 0.7 nm (at 1308 nm) were observed at 2.7 and 2 mA for filters with 20- and 40- $\mu\text{m}$  cavities (Figs. 6 and 7), respectively.

It is interesting to note that for higher injected currents, we were not able to observe larger blue shifts. We believe that this is due to heating effects, as the thermally induced refractive-index change has the opposite sign to that of the carrier-induced shift.

This heating effect is further explored in Fig. 7, which shows refractive-index shift versus injected current. The index shift is negative at first, indicative of a carrier-induced effect, but then reverses direction, following the positive index change of the thermo-optic effect. We typically observe laser operation at the changeover point, which explains the observed trend. Once a device reaches laser threshold, the gain is clamped, so no further index change due to electrooptic effects is obtained. Increasing the current further does increase the temperature of the device, however, so thermo-optic effects then dominate above threshold.

The low laser threshold, while being noteworthy in its own right, is disadvantageous for tuning purposes, because it prevents any further tuning through C-I. It does, however, give an easy route to extracting the thermal properties of the device. By converting current to dissipated power ( $P_D$ ) in Fig. 7, the slope of the curve ( $>2$  mA) gives the product of thermal resistance and the thermo-optic coefficient ( $\partial n/\partial T$ ). Thus, knowing  $\partial n/\partial T$  for InGaAsP from the literature (typically around  $2 \times 10^{-4} \text{ K}^{-1}$  [16]), the thermal resistance ( $Z_T$ ) of the device is calculated to be 0.2 K/mW. We used the formula  $\Delta T = Z_T P_D$  from [17].

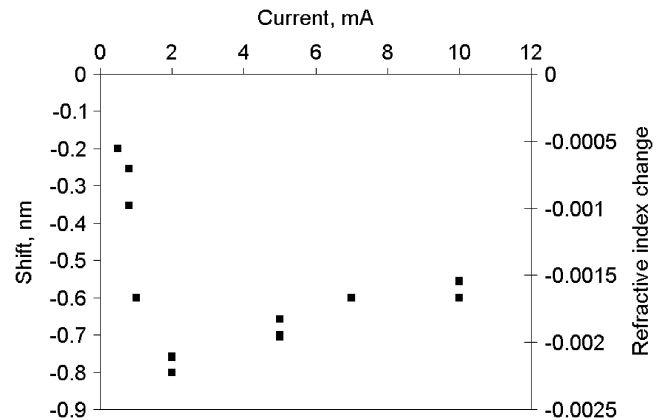


Fig. 7. Carrier-induced refractive-index changes in a 40- $\mu\text{m}$  cavity filter (at 1309-nm wavelength). The modal refractive-index change is given. A pronounced thermally induced red shift appears for currents above 2 mA.

For comparison, a thermal resistance of 0.4 K/mW was calculated for the device with the 20- $\mu\text{m}$ -long cavity. Interestingly, both of these thermal resistances are less than half of their calculated values, which are 0.5 and 1 K/mW for 40- and 20- $\mu\text{m}$ -long cavities, respectively. We believe that this is due to heat dissipation by the top contact pad that had been deliberately made oversized, thereby acting as a “cooling fin” [18].

The largest electrooptic tuning was observed for the smaller cavity, in spite of its larger thermal resistance. This is a consequence of its higher lasing threshold that delays the point at which the thermal effect takes over.

Pulsed currents (10- $\mu\text{s}$  pulsewidth for a 1000  $\mu\text{s}$  period) were used in order to minimize the heating problem. As a consequence, a higher blue shift of 1.9 nm was obtained for an injection current of 2.69 mA for the filter with a 20- $\mu\text{m}$ -long cavity. The difference between this value and the 1.5-nm blue shift obtained in the direct current (dc) measurement, described previously, agrees well with the red shift (0.3 nm) caused by heating (calculated using the experimental thermal resistance of 0.4 K/mW measured previously).

The rate of change of the transmission peak with current shown in Fig. 7 is  $(\Delta\lambda/I) = 0.36 \text{ nm/mA}$ . For comparison, this value exceeds the value of  $\sim 0.09 \text{ nm/mA}$  for InGaAsP–InP F–P cavity reported by Tsang *et al.* [19] and is of the same order as that reported by Djordjev *et al.* [2].

## VII. QCSE AND C-I COMPARISON

Table II shows a comparison between the experimentally achieved filter transmission peaks shifts induced via QCSE and C-I.

As one can see from the Table II, the observed shifts obtained with the different methods are in fact very close (a QCSE red shift of 1.2 and a C-I blue shift of 1.5 nm). However, the data presented in Table II for QCSE-induced shift is data for an average device, and using the experimentally measured electrooptic parameter of  $\eta = 14 \times 10^{-5} \text{ meV cm}^2 \text{ kV}^{-2}$  (achieved for the best device), we can predict a QCSE-induced red shift for an applied voltage of 50 kV/cm and a detuning of  $\Delta\omega = 40 \text{ meV}$  of 3 nm. Furthermore, QCSE is faster than C-I as there is no need to sweep carriers out of the QWs, and there are no carrier-related

TABLE II  
COMPARISON BETWEEN QCSE- AND C-I-BASED  
TUNABLE FILTERS, PRESENTED IN THIS PAPER

Parameters	QCSE	Carrier-Injection
Number of QWs	10	5
Modal confinement factor, %	6	8
Cavity length, $\mu\text{m}$	20	20
Shift, nm	1.2	1.5
Detuning from the band-edge, nm	70	40
Electric field, kV/cm	62	50
$\Delta n/\Delta k$	20	26
Material index change (quantum wells)	0.05	0.046

heating effects. On the other hand, QCSE-related absorption losses are higher and increase rapidly compared with C-I. This can badly compromise filter performance (thereby reducing the  $Q$  factor), especially at high electric fields ( $>100$  kV/cm).

### VIII. CONCLUSION

Deeply etched tunable filters in InP-based material with five and ten quaternary quantum wells (QWs) were designed and successfully fabricated. A full-width at half-maximum (FWHM) of less than 2 nm and a free spectral range (FSR) of 12 nm was experimentally achieved for a filter with a 20- $\mu\text{m}$  cavity. At an applied voltage of 6 V (37.5 kV/cm), we observed a red shift of 1.2 nm of the filter resonance wavelength at 1320 nm for ten QWs quantum-confined Stark effect (QCSE) material. This shift corresponds to an efficiency  $\Delta n/E = 820 * 10^{-12}$  m/V.

It is believed that the results from the best device illustrate the potential of this material and design and that other devices were handicapped by imperfections in the problematic T-contact. Thus, for an increased applied field up to 50 kV/cm at a wavelength of 1265 nm, it is predicted that the red shift may reach 5 nm (see (2)), though, with the penalty of increased absorption losses. However, it should be noted that most of this absorption loss occurs in the access waveguides—compare the heights of the unshifted peaks at 1265 and 1285 nm in Fig. 4. (Large shifts of 1.6 nm of low- $Q$  peaks were, in fact, obtained). By pumping these waveguides, this loss may be compensated for, giving very high performance. Furthermore, as has recently been proposed, the use of chopped (coupled) QWs can give up to two times higher QCSE red shifts [20]. With a slight increase of strain, this chopped QW material may also be used for polarization independent switching.

Using carrier injection (C-I), similar shifts of 1.5 nm (dc) and 1.9 nm (pulsed) were achieved for the 5 QWs' material, while only 6 mW of power was consumed. A design with large contact pads (relative to the size of the cavities) allowed the reaching of

relatively small thermal resistances of 0.2 and 0.4 K/mW for filters with 20- and 40- $\mu\text{m}$  cavities, respectively. Larger shifts may be achieved by shifting the reflectivity peak of the mirrors, in order to suppress laser action at the gain peak, hence increasing the tuning range.

Finally, the modest shifts of 1 to 2 nm demonstrated here emphasize the difficulties experienced by many researchers in obtaining substantial wavelength shifts for microphotonic devices. While relatively large *material* index changes ( $\Delta n \approx 0.05$  or more) can in principle be achieved, obtaining these as *modal* index changes in a real device, taking losses and heating effects into account, is not easy. The heating effects observed in this paper also emphasize the difference between III-V and silicon-on-insulator (SOI)-based devices, whereby the III-V-based structures offer advantages in terms of both reducing the thermal impedance and achieving higher electronic shifts due to band filling.

Overall, the limitations and opportunities for III-V semiconductor-based tunable microphotonic circuit elements have been emphasized by analyzing the operation of compact tunable filters in the 1.3- $\mu\text{m}$  wavelength regime.

### ACKNOWLEDGMENT

The authors would like to thank G. Robb, D. H. Brown, and T. Karle for their help with experiments.

### REFERENCES

- [1] T. A. Ibrahim, W. Cao, Y. Kim, J. Li, J. Goldhar, P.-T. Ho, and C. H. Lee, "Lightwave switching in semiconductor microring devices by free carrier injection," *J. Lightw. Technol.*, vol. 21, no. 12, pp. 2997–3003, Dec. 2003.
- [2] K. Djordjevic, S.-J. Choi, S.-J. Choi, and P. D. Dapkus, "Microdisk tunable resonant filters and switches," *IEEE Photon. Technol. Lett.*, vol. 14, no. 6, pp. 828–830, Jun. 2002.
- [3] C. A. Barrios, V. R. Almeida, R. R. Panepucci, B. S. Schmidt, and M. Lipson, "Compact silicon tunable Fabry-Pérot resonator with low power consumption," *IEEE Photon. Technol. Lett.*, vol. 16, no. 2, pp. 506–508, Feb. 2004.
- [4] R. Ferrini, B. Lombardet, B. Wild, R. Houdre, S. Olivier, H. Benisty, A. Djoudi, L. Legouezigou, S. Hubert, S. Sainson, J.-P. Chandouineau, S. Fabre, F. Pommereau, and G.-H. Duan, "Optical characterization of 2-D InP-based photonic crystals fabricated by inductively coupled plasma etching," *Electron. Lett.*, vol. 38, pp. 962–964, Aug. 2002.
- [5] M. V. Kotlyar, L. O'Faolain, R. Wilson, and T. F. Krauss, "High-aspect-ratio chemically assisted ion-beam etching for photonic crystals using a high beam voltage-current ratio," *J. Vac. Sci. Technol. B, Microelectron. Process. Phenom.*, vol. 22, pp. 1788–1791, Jul. 2004.
- [6] M. V. Kotlyar, T. Karle, M. D. Settle, L. O'Faolain, and T. F. Krauss, "Low-loss photonic crystal defect waveguides in InP," *Appl. Phys. Lett.*, vol. 84, pp. 3588–3590, May 2004.
- [7] T. F. Krauss and R. M. De La Rue, "Optical characterization of waveguide based photonic microstructures," *Appl. Phys. Lett.*, vol. 68, pp. 1613–1615, Mar. 1996.
- [8] D. A. B. Miller, J. S. Weiner, and D. S. Chemla, "Electric-field dependence of linear optical properties in quantum well structures: Waveguide electroabsorption and sum rules," *IEEE J. Quantum Electron.*, vol. 22, no. 9, pp. 1816–1830, Sep. 1986.
- [9] J. E. Zucker and T. L. Henderickson, "Electro-optic phase modulation in GaAs/AlGaAs quantum well waveguides," *Appl. Phys. Lett.*, vol. 52, pp. 945–947, Mar. 1988.
- [10] B. R. Bennett, R. A. Soref, and J. A. Del Alamo, "Carrier-induced change in refractive index of InP, GaAs, and InGaAsP," *IEEE J. Quantum Electron.*, vol. 26, no. 1, pp. 113–122, Jan. 1990.
- [11] K. Frojdh and S. Marcinkevicius, "Interwell carrier transport in InGaAsP multiple quantum well laser structures," *Appl. Phys. Lett.*, vol. 69, pp. 3695–3697, Dec. 1996.

- [12] W. Bogaerts, P. Bienstman, D. Taillaert, R. Baets, and D. De Zutter, "Out-of-plane scattering in 1-D photonic crystal slabs," *Optic. Quantum Electron.*, vol. 34, pp. 195–203, Jan./Mar. 2002.
- [13] J. E. Zucker, I. Bar-Joseph, B. I. Miller, U. Koren, and D. S. Chemla, "Quaternary quantum wells for electro-optic intensity and phase modulation at 1.3 and 1.55  $\mu\text{m}$ ," *Appl. Phys. Lett.*, vol. 54, pp. 1989–1991, Jan. 1989.
- [14] R. Grover, T. A. Ibrahim, S. Kanakaraju, L. Lucas, L. C. Calhoun, and P.-T. Ho, "A tunable GaInAsP–InP optical microring notch filter," *IEEE Photon. Technol. Lett.*, vol. 16, no. 2, pp. 467–469, Feb. 2004.
- [15] M. V. Kotlyar, L. O'Faolain, A. Krysa, and T. F. Krauss, "Electrically tunable multi-quantum-well InGaAsP–InGaAsP microphotonic filter," *IEEE Photon. Technol. Lett.*, vol. 17, no. 4, pp. 837–839, Apr. 2005.
- [16] F. G. D. Corte, G. Cocorullo, M. Iodice, and I. Rendina, "Temperature dependence of the thermo-optic coefficient of InP, GaAs, and SiC from room temperature to 600 K at the wavelength of 1.5  $\mu\text{m}$ ," *Appl. Phys. Lett.*, vol. 77, pp. 1614–1616, Sept. 2000.
- [17] L. A. Coldren and S. W. Corzine, *Diode Lasers and Photonic Integrated Circuits*, ser. Wiley Series in microwave and optical engineering. New York: Wiley, 1995, p. 56.
- [18] K. P. Pipe and R. J. Ram, "Comprehensive heat exchange model for a semiconductor laser diode," *IEEE Photon. Technol. Lett.*, vol. 15, no. 4, pp. 504–506, Apr. 2003.
- [19] H. K. Tsang, M. W. Mak, L. Y. Chan, J. B. D. Soole, C. Youtsey, and I. Adesida, "Etched cavity InGaAsP/InP waveguide Fabry–Pérot filter tunable by current injection," *J. Lightw. Technol.*, vol. 17, no. 10, pp. 1890–1895, Oct. 1999.
- [20] B. H. Dorren, A. Yu. Silov, M. R. Leys, D. M. H. Dukers, J. E. M. Haverkort, D. H. Maat, Y. Zhu, F. H. Groen, and J. H. Wolter, "A chopped quantum-well polarization independent interferometric switch at 1.53  $\mu\text{m}$ ," *IEEE J. Quantum Electron.*, vol. 36, no. 3, pp. 317–324, Mar. 2000.

**Maria V. Kotlyar** received the first-class honors diploma in physics from Samara State University, Samara, Russia, in 2001. She is currently working toward the Ph.D. degree on tunable photonic-crystal devices in InP-based material at the University of St. Andrews, Fife, U.K.

**Liam O'Faolain** received the B.Sc. degree (with honors) in physics from the National University of Ireland, Cork, in 2001. He is currently working toward the Ph.D. degree on mode-locked semiconductor lasers diodes at the University of St. Andrews, Fife, U.K.

**Andrey B. Krysa** received the M.Sc. degree from the Moscow Engineering Physics Institute, Moscow, Russia, in 1990 and the Ph.D. degree in solid-state physics from the Lebedev Physical Institute of Russian Academy of Sciences, Moscow, Russia, in 1997.

In 1995, he joined the Department of Optoelectronics at the Lebedev Physical Institute as a Research Associate. From 1999 to 2000, he worked at the Institut für Halbleitertechnik, RWTH Aachen, Aachen, Germany, as a Humboldt Research Fellow on the problem of ZnSe homoepitaxial growth by metal organic vapor phase epitaxy (MOVPE). Since joining the Engineering and Physical Sciences Research Council (EPSRC) National Centre for III–V Technologies, University of Sheffield, Sheffield, U.K., in 2001, he has been engaged in the MOVPE of Al–Ga–In–As–P-based structures.

**Thomas F. Krauss** received the Ph.D. degree from Glasgow University, Glasgow, U.K., where his graduate studies focused on the topic of monolithic semiconductor-ring lasers, and he was the first to demonstrate continuous-wave operation as well as optoelectronic integrated circuit (OEIC) functionality.

He has been involved in optoelectronics research for the 15 years since working on Ti–LiNbO<sub>3</sub> waveguides at IBM, Yorktown Heights, NY, from 1987 to 1988. As a Royal Society Research Fellow, he then initiated the field of semiconductor photonic crystals in the United Kingdom (1993) and has since established a reputation worldwide, as evidenced by the large number of invited talks he presents at an international level (10–12 per year). In 1997, he spent a year at the California Institute of Technology, Pasadena, to work on efficient photonic crystal-based light emitters. In 2000, he accepted a Personal Chair in optoelectronics at the School of Physics and Astronomy, University of St. Andrews, Fife, U.K., and established a microphotonic and photonic-crystal research group (currently 15 members) and semiconductor microfabrication laboratory. He is a Grant Holder of several U.K. research projects and was Coordinator of the FP5-IST research project "Photonic Integrated Circuits Using Photonic Crystals" (PICCO), involving seven academic and industrial partners from Belgium, Denmark, Italy, and the United Kingdom.

Dr. Krauss was elected a Fellow of the Institute of Physics in 2001 and the Royal Society of Edinburgh in 2002.